Journal of Materials Chemistry C

PAPER

View Article Online
View Journal | View Issue

Cite this: J. Mater. Chem. C, 2020, 8, 602

Double-twist pyridine–carbonitrile derivatives yielding excellent thermally activated delayed fluorescence emitters for high-performance OLEDs†

Jiafang Li,[a] Wen-Cheng Chen,[b] He Liu,*[a] Zhanxiang Chen,[c] Danyang Chai,[a] Chun-Sing Lee*[b] and Chuluo Yang*[ac]

Received 29th September 2019,
Accepted 17th November 2019

DOI: 10.1039/c9tc05340a

rsc.li/materials-c

Possessing high photoluminescence quantum yield (PLQY) and fast reverse intersystem crossing (RISC) process are critical for obtaining efficient thermally activated delayed fluorescence (TADF) emitters. Herein, two donor–spacer–acceptor molecules, namely, 4-(4-(9,9-dimethylacridin-10(9*H*)-yl)phenyl)-2,6-dimethylpyridine-3,5-dicarbonitrile (Me-DMAC) and 4-(4-(10*H*-phenoxazin-10-yl)phenyl)-2,6-dimethylpyridine-3,5-dicarbonitrile (Me-PXZ), were developed *via* a double-twist design strategy. The large hindrance induces a twisted geometry, leading to small ΔE_{ST} values and fast RISC processes. The time-resolved photophysical measurements revealed the TADF emissions of these pyridine-3,5-dicarbonitrile-based molecules in doped thin films. High external quantum efficiency (EQE) values of 25.8% and 21.1% were achieved in organic light-emitting diodes (OLEDs) using green Me-DMAC and yellow Me-PXZ dyes, respectively, as emitters.

Introduction

Manipulating the excited states to completely utilize the electrically generated excitons, including singlet (S) and triplet (T) excitons in the ratio 1 : 3,[1] has always been a formidable challenge in the history of organic light-emitting diodes (OLEDs).[2–14] One of the most attractive ways is to manage pathways between the S and T excited states.[15–20] Among the efforts made by worldwide researchers, several mechanisms that can completely harvest both S and T excitons have been proposed. By enhancing the spin–orbit coupling by introducing heavy metal elements, the lowest excited state (T_1) can radiatively decay *via* phosphorescence, leading to 100% internal quantum yield in OLEDs.[15,16] With regard to pure organic molecules, an alternative pathway can be opened by minimizing the energy difference (ΔE_{ST}) between the lowest S (S_1) and T (T_1) excited states, yielding an efficient reverse intersystem crossing (RISC) process. This is referred to as thermally activated delayed fluorescence (TADF).[17,18] By effecting an intricate molecular design, RISC pathways can also be established between the higher excited states (T_m–S_n), which is described by the "hot exciton" mechanism featuring neglectable delayed fluorescence.[19,20] Among all these methods, TADF has attracted considerable attention recently. One reason for this is that TADF emitters can be easily constructed at a lower cost since the selection of a pure organic donor and acceptor building blocks are infinite and inexpensive. At an early stage, TADF emitters have already broken the 20% external quantum efficiency limit of ordinary fluorescent OLEDs.[18] Recently, an ultrahigh external quantum efficiency exceeding 38% in the blue region was achieved *via* the combination of boron acceptors and indolocarbazole donor,[21] which further demonstrates its potential.

In general, a small ΔE_{ST} value is required to ensure effective RISC from electrogenerated triplet excitons to S (usually S_1). Meanwhile, a sufficiently high photoluminescence quantum yield (PLQY) of S_1 is also needed to maximize the conversion of S excitons into photons. The rate constant of RISC (k_{RISC}) is expressed as $k_{RISC} = \sim A \times \exp(-\Delta E_{ST}/k_B T)$, where A is the preexponential factor, k_B is the Boltzmann constant, and T is the temperature.[22] Therefore, a high k_{RISC} value can be achieved by achieving a sufficiently small ΔE_{ST} value. In conventional molecular design, a reduced ΔE_{ST} value can be achieved by minimizing the overlap between the highest occupied

[a] Shenzhen Key Laboratory of Polymer Science and Technology, Guangdong Research Center for Interfacial Engineering of Functional Materials, College of Materials Science and Engineering, Shenzhen University, Shenzhen 518060, People's Republic of China. E-mail: clyang@szu.edu.cn, liuhe001@szu.edu.cn

[b] Center of Super-Diamond and Advanced Films (COSDAF) and Department of Chemistry, City University of Hong Kong, Kowloon, Hong Kong SAR 999077, P. R. China. E-mail: C.S.Lee@cityu.edu.hk

[c] Department of Chemistry, Hubei Key Lab on Organic and Polymeric Optoelectronic Materials, Wuhan University, Wuhan 430072, People's Republic of China. E-mail: clyang@whu.edu.cn

† Electronic supplementary information (ESI) available. See DOI: 10.1039/c9tc05340a

molecular orbital (HOMO) and lowest unoccupied molecular orbital (LUMO) by connecting the electron donor and electron acceptor with a large torsion angle. However, small overlaps between the HOMO and LUMO generally tend to decrease the value of the radiative decay rate (k_r) and oscillator strength between the S_1 and ground state (S_0),[23] thereby limiting PLQY. Consequently, the external quantum efficiency (EQE) of devices can be seriously decreased.[24] The tradeoff between high k_r/PLQY and fast RISC process demands a careful molecular design and smarter choices of donor and acceptor units.

The cyano group (CN) with a strong electron-withdrawing effect and short conjugation length has been a popular acceptor building block since the early design of TADF emitters. The star-shape 2,4,5,6-tetra(9*H*-carbazol-9-yl)isophthalonitrile (4CzIPN) molecule is the first reported green TADF emitters, reaching EQE higher than 20%.[18] Extensive research has been conducted afterward, leading to EQE as high as 31.2%.[25] The derivatives of 4CzIPN as well as other materials containing CN-benzene building blocks also exhibit excellent electroluminescent (EL) performance.[26–30] As compared to the CN-benzene unit, the CN-pyridine group has drawn lesser attention for application in TADF emitters, but most of the reported compounds perform well in EL devices. Huang's group reported a 4-CN-pyridine-based green emitter, namely, 4CzCNPy, with a structure similar to that of 4CzIPN, achieving EQE value of 19.7%.[31] Wong's,[32] Kido's,[33] and Zhang's[34] groups developed CN- and diCN-pyridine derivatives, reaching EQE values of 29.2%, 22.7%, and 21.2%, respectively. Su and coworkers developed 3,5-diCN-pyridines, possessing high exciton utilization efficiency even with large ΔE_{ST}.[35] Recently, our group reported 3,5-diCN-pyridine derivatives, exhibiting the maximum EQE of 20%.[36] Both high k_r/PLQY and fast RISC process can be established in these systems. Further exploring CN-pyridine-based TADF emitters would facilitate insights into and the construction of more practical materials.

Herein, two molecules containing donor–spacer–acceptor double-twist structure called 4-(4-(9,9-dimethylacridin-10(9*H*)-yl)phenyl)-2,6-dimethylpyridine-3,5-dicarbonitrile (Me-DMAC) and 4-(4-(10*H*-phenoxazin-10-yl)phenyl)-2,6-dimethylpyridine-3,5-dicarbonitrile (Me-PXZ) with 9,9-dimethyl-9,10-dihydroacridine (DMAC) and 10*H*-phenoxazine (PXZ) (Fig. 1a) as the corresponding donors were designed. Considering the requirement of a fast RISC process, 3,5-diCN-pyridine connected *via* the 4 position was adopted as the acceptor. Two adjacent CN groups could induce large hindrance that could resulted in more twisted geometry. Further, a benzene ring introduced as a spacer between the donor and acceptor could further enlarge the overlap between the HOMO and LUMO. The double twists between the donor–spacer and acceptor–spacer can ensure small ΔE_{ST}. The rational designs of Me-DMAC and Me-PXZ can yield excellent OLEDs with maximum EQE values of 25.8% and 21.1%, respectively.

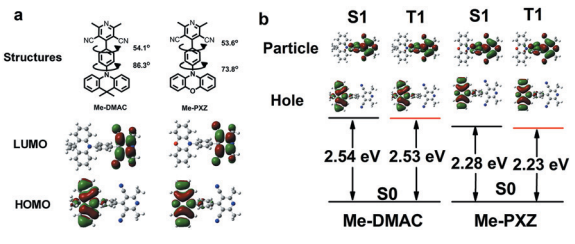

Fig. 1 Molecular structures and DFT simulation of ground and excited states of Me-DMAC and Me-PXZ. (a) Molecular structures and distribution of HOMO and LUMO. (b) NTO distributions of S_1 and T_1 of Me-DMAC and Me-PXZ.

Results and discussion

Synthesis and thermal properties

Me-DMAC and Me-PXZ were synthesized through Buchwald–Hartwig coupling reactions between 4-(4-bromophenyl)-2,6-dimethylpyridine-3,5-dicarbonitrile (Me-Br) and DMAC or PXZ in good yields (Scheme S1, ESI†). The compounds were fully identified by ^{1}H NMR, ^{13}C NMR spectroscopy, MALDI-TOF, and elemental analysis. Thermal gravimetric analysis (TGA) showed the decomposition temperatures (T_d) at about 282 °C and 298 °C with 5% loss of weight (Fig. S1(a), ESI†). In addition, the glass transition temperatures were not found for both these materials during the second heating (differential scanning calorimetry curve, Fig. S1(b), ESI†), which demonstrates their good thermal stability for evaporating deposition OLED devices.

Theoretical simulations

To validate our design, density functional theory (DFT) simulation was performed under the B3LYP-D3(BJ)/def2-SVP and PBE0/def2-SVP levels to optimize their ground and excited states, respectively. The oscillator strengths (f) were calculated by using time-dependent DFT (TDDFT) calculations at the PBE0/def2-SVP level with the nuclear ensemble approach.[37] As shown in Fig. 1a, LUMOs of both the molecules were entirely located on the acceptor unit. This may be attributed to two reasons. First, the large hindrance of CN breaks the conjugation. Second, the strong electron-withdrawing effect of CN pins LUMO on the acceptor unit. Meanwhile, the HOMOs are mainly spread on the donor unit with a small portion remaining on the central benzene. The electron-donating effects of nitrogen shares a part of the electron with the adjacent benzene. The complete separation of HOMO and LUMO ensures a small ΔE_{ST} value, which is also proven in the natural transition orbital (NTO) analysis, as shown in Fig. 1b. Both Me-DMAC and Me-PXZ possess small ΔE_{ST} values of 0.01 and 0.05 eV, respectively. Such small ΔE_{ST} values facilitate efficient RISC. The calculated f values of Me-DMAC and Me-PXZ are 0.007230 and 0.006414 (Table S1, ESI†), respectively, which suggest their high PLQY values.

Photophysical properties

To experimentally validate the above speculation, UV-vis absorption, fluorescence (Fl), and phosphorescence (Ph) tests were performed. The spectra for 1,3-bis(*N*-carbazolyl)benzene (mCP) film (10 wt%) and in dilute toluene are shown in Fig. 2 and Fig. S3 (ESI†), respectively, and detailed data are summarized in Table 1.

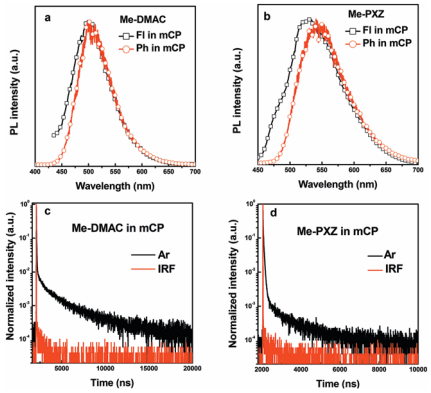

Fig. 2 Fluorescence and phosphorescence spectra (at 77 K) in mCP-doped film (10 wt%) of (a) Me-DMAC and (b) Me-PXZ obtained *via* spin-coating. Transient decay spectra of (c) Me-DMAC and (d) Me-PXZ in mCP-doped film (10 wt%) under oxygen-free condition.

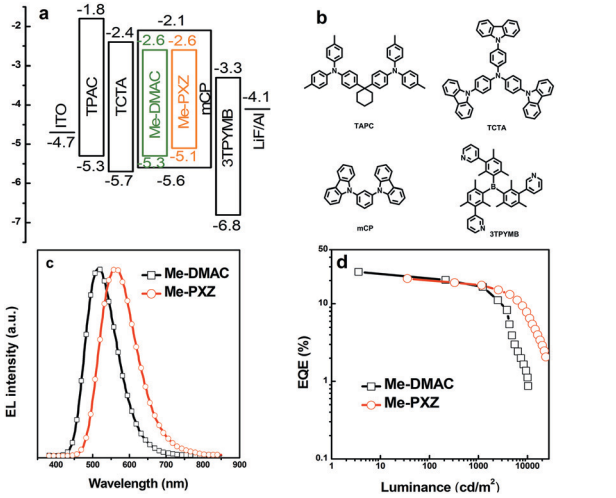

Fig. 3 (a) Energy diagram of the doped device. (b) Chemical structures of the materials used in the device, fabrication. (c) EL spectra of the devices based on Me-DMAC and Me-PXZ. (d) EQE–*L* characteristics of the devices.

UV-vis spectra in dilute toluene exhibit weak charge transfer (CT) absorptions at around 381 and 412 nm for Me-DMAC and Me-PXZ, respectively. As demonstrated in the CV results (Fig. S4, ESI†), PXZ possesses stronger electron-donating ability than that of DMAC. Therefore, a more efficient CT excited state is formed when connected with an acceptor, leading to redshifts in the absorption and emission. Dual emissions are found in these two materials. Taking Me-DMAC as an example, emissions with short (444 nm) and long (542 nm) wavelengths may be attributed to the so-called "quasi-axial" (QA) and "quasi-equatorial" (QE) conformations, respectively.[38,39] The QE conformation possesses more planar geometry that leads to low-lying energy and efficient CT. The theoretical geometries of QA and QE conformations of Me-DMAC and Me-PXZ were calculated, as shown in Fig. S5 (ESI†). The Fl and Ph spectra were also obtained in doped mCP films (10 wt%) to evaluate the properties in the solid state toward device applications. The Fl emissions are located at 499 and 529 nm for Me-DMAC and Me-PXZ, respectively. The shoulder due to QA configuration is found in Me-PXZ films. The energy levels of S1 and T1 calculated from the onset of the spectra are 2.85 (2.73) and 2.64 (2.55) eV for Me-DMAC (Me-PXZ), respectively. Therefore, the ΔE_{ST} values for Me-DMAC and Me-PXZ were estimated to be 0.12 and 0.09 eV, respectively. When compared with the theoretical results, the slightly larger ΔE_{ST} values prove that a certain degree of HOMO–LUMO overlap does exist. In addition, both Me-DMAC and Me-PXZ possess high absolute PLQY values of 96% and 71% in mCP-doped films, respectively. Such high PLQY values improve device efficiency.

To further understand the photophysical properties, transient photoluminescence (PL) measurement was carried out in mCP (10 wt%)-doped films and in toluene (10^{-4} M). As shown in Fig. 2c, d, and Fig. S3 (ESI†), the PL lifetimes of Me-DMAC and Me-PXZ under Ar atmosphere clearly exhibit two components: one is the prompt portion from direct S_1 to S_0 transition and the other is the delayed portion related to recursive S_1 to S_0 transition. The delayed PL portion in dilute toluene is quenched after bubbling

Table 1 Photophysical and electrochemical data of Me-DMAC and Me-PXZ

	HOMO[a,b] (eV)	LUMO[a,c] (eV)	S_1[a,d] (eV)	T_1[a,d] (eV)	ΔE_{ST}[a,d] (eV)
Me-DMAC	−5.20/−5.28	−2.38/−2.57	2.54/2.85	2.53/2.73	0.01/0.12
Me-PXZ	−4.97/−5.09	−2.41/−2.61	2.29/2.64	2.24/2.55	0.05/0.09

[a] Results from theoretical simulations under the B3LYP-D3(BJ)/def2-SVP and PBE0/def2-SVP levels for the ground and excited states, respectively. [b] Calculated from the onset of cyclic voltammetry (Fig. S4, ESI). [c] Calculated from the following equation: LUMO = HOMO + E_g, where E_g denotes the estimated value from absorption in dilute toluene. [d] Estimated from the onset of fluorescence and phosphorescence spectra of the mCP-doped film (10 wt%).

Table 2 Photophysical data of Me-DMAC and Me-PXZ in the doped film (10 wt% in mCP) at room temperature

	τ_p (ns)	τ_d (μs)	Φ_{PL} (%)	Φ_p (%)	Φ_d (%)	k_r (10^7 s^{-1})	k_{ISC} (10^7 s^{-1})	k_{RISC} (10^6 s^{-1})
Me-DMAC	22.9	2.7	96	20.0	76.0	0.90	3.57	1.70
Me-PXZ	24.8	1.0	71	47.8	23.2	1.95	1.34	1.47
4CzIPN[a]	16.0	4.6	82	—	—	0.63	5.60	2.03

τ_p: lifetime of the prompt component; τ_d: lifetime of the delayed component; Φ_{PL}: PLQY in the mCP-doped film; Φ_p: quantum yield of the prompt component; Φ_d: quantum yield of the delay component; k_r, k_{ISC}, and k_{RISC} represent the rate constant of radiative, ISC, and RISC, respectively. [a] Results of 4CzIPN was tested in CBP (4,4′-*N*,*N*′-dicarbazole-biphenyl) (6 wt%) by Masui *et al.*[40]

Table 3 Electroluminescence characteristics of the devices

Emitter	V_{on}[a] (V)	λ_{EL}[b] (nm)	CIE[b] (x, y)	Current eff.[b,c] (cd A^{-1})	Power eff.[b,c] (lm W^{-1})	EQE[b,c] (%)
Me-DMAC	3.2	517	(0.28, 0.51)	59.3, 53.6	46.6, 39.2	25.8, 18.2
Me-PXZ	3.0	562	(0.44, 0.53)	54.4, 53.5	48.2, 37.2	21.1, 18.1

[a] Voltage at 1 cd m^{-2}. [b] Measured at 1000 cd m^{-2}. [c] Efficiencies at maximum and 1000 cd m^{-2}, respectively.

with O_2, indicating this process involves RISC from the T excited state. As the PL transient decay curves can be fitted well with double-exponential functions, the prompt (τ_p) and delayed (τ_d) fluorescent lifetimes together with the PLQY of prompt (Φ_p) and delayed (Φ_d) components can be determined. The rate constants of prompt (k_p) and delayed (k_d) fluorescence, radiative decay (k_r), and ISC (k_{ISC}) and RISC (k_{RISC}) processes can be estimated (equations are listed in the ESI†). The rate constants of different kinetic processes are listed in Table 2. High k_r and k_{RISC} values of $\sim 10^7$ and $\sim 10^6$ could be achieved. Both these compounds possessed k_{RISC} values of the same order of magnitude as those of 4CzIPN.[19,40] Considering the high utilization of T excitons of 4CzIPN, our molecules should perform in a similar manner. In short, these photophysical properties suggest that Me-DMAC and Me-PXZ possess high PLQY and exhibit a fast RISC process.

EL properties

As theoretically predicted and experimentally revealed, both Me-DMAC and Me-PXZ could yield excellent device performances. OLED devices with a structure of ITO/TPAC (40 nm)/TCTA (10 nm)/mCP:10 wt% emitters (20 nm)/3TPYMB (55 nm)/LiF (1 nm)/Al (100 nm) were fabricated to seek validation. Here, 1,1-bis[4-[*N*,*N*′-di(*p*-tolyl)amino]phenyl]cyclohexane (TAPC) and 4,4′,4″-tri(9-carbazoyl)triphenylamine (TCTA) were used as the hole-transporting layer, and mCP served as the host material for Me-DMAC and Me-PXZ. Further, tri[3-(3-pyridyl)mesityl]borane (3TPYMB) was employed as the electron-transporting layer. The energy level diagram of the devices, EL spectrum, external quantum efficiency–luminescence (EQE–*L*), and current density–voltage–luminescence (*J*–*V*–*L*) curves are shown in Fig. 3 and Fig. S6 (ESI†). The key data of the devices are listed in Table 3. The single-peak emission of the EL spectrum indicates the absence of the QA configuration in the vacuum deposition process and efficient energy transfer from the host to the TADF emitters. Both these devices exhibit high current efficiency (CE), power efficiency (PE), and EQE. Me-PXZ endowed yellow devices with maximum CE (CE_{max}), PE (PE_{max}), and EQE (EQE_{max}) values of 54.4 cd A^{-1}, 48.2 lm W^{-1}, and 21.1%, respectively. Further, Me-DMAC performed better, where the CE_{max}, PE_{max}, and EQE_{max} values were 59.3 cd A^{-1}, 46.6 lm W^{-1}, and 25.8%, respectively. Neither of the devices employs the light out-coupling process. The utilizations of excitons were estimated from the equation UE = EQE/(PLQY·η_{out}), where η_{out} is the out-coupling efficiency ($\sim$0.3); the efficiencies were calculated as 90% and 99%. Such high efficiencies for these devices can be attributed to the excellent PLQY, fast RISC process, and intelligent selection of the host material and design of the device structures. Me-PXZ-based devices show lower roll-off of 14% at 1000 cd m^{-2} than that of Me-DMAC (29%), indicating that the shorter lifetime of the delayed component could alleviate efficiency roll-off.

The excellent EL performances of both Me-DMAC and Me-PXZ demonstrate that high PLQY together with fast RISC process are critical for fabricating efficient TADF emitters. This also proves the rationality of the double-twist design strategy and the suitable choice of donor and acceptor. We hope that these results can provide guidelines for further molecular design.

Conclusions

In summary, we have developed two donor–spacer–acceptor-type double-twist TADF emitters for Me-DMAC and Me-PXZ. The underlying TADF properties of these materials were investigated by time-resolved photophysical measurements, together with TDDFT calculations. The two emitters of Me-DMAC and Me-PXZ exhibited TADF emissions with very high PLQY values of up to 96% in doped thin films. As a result, devices doped with the mCP host yielded EQE_{max} values of 25.8% and 21.1% (for Me-DMAC and Me-PXZ, respectively), which are among the best available results. The excellent device performance demonstrates that the double-twist design strategy is effective in yielding desirable TADF emitters.

Conflicts of interest

There are no conflicts to declare.

Acknowledgements

This work was supported by the National Natural Science Foundation of China (No. 51803125 and 91833304), Shenzhen Peacock Plan (KQTD20170330110107046), Science and Technology Innovation Commission of Shenzhen (JCYJ20180507182244027) and Natural Science Foundation of SZU (No. 2018002). The numerical calculations in this paper have been done on the supercomputing system in the Supercomputing Center of Wuhan University.

Notes and references

1 M. A. Baldo, M. E. Thompson and S. R. Forrest, *Phys. Rev. B: Condens. Matter Mater. Phys.*, 1999, **60**, 422–428.
2 Y. Cao, I. D. Parker, G. Yu, C. Zhang and A. J. Heeger, *Nature*, 1999, **397**, 414–417.
3 A. S. Dhoot, D. S. Ginger, D. Beljonne, Z. Shuai and N. C. Greenham, *Chem. Phys. Lett.*, 2002, **360**, 195–201.

4 Y. Ma, Z. Houyu, J. Shen and C. Che, *Synth. Met.*, 1998, **94**, 245–248.
5 M. A. Baldo and S. R. Forrest, *Nature*, 1998, **395**, 151–154.
6 C. J. Chiang, A. Kimyonok, M. K. Etherington, G. C. Griffiths, V. Jankus, F. Turksoy and A. P. Monkman, *Adv. Funct. Mater.*, 2013, **23**, 739–746.
7 H. Uoyama, K. Goushi, K. Shizu, H. Nomura and C. Adachi, *Nature*, 2012, **492**, 234–238.
8 W. Zeng, T. Zhou, W. Ning, C. Zhong, J. He, S. Gong, G. Xie and C. Yang, *Adv. Mater.*, 2019, **1901404**, 1–8.
9 K. Wu, T. Zhang, L. Zhan, C. Zhong, S. Gong, Z. H. Lu and C. Yang, *Adv. Opt. Mater.*, 2016, **4**, 1558–1566.
10 K. Wu, T. Zhang, L. Zhan, C. Zhong, S. Gong, N. Jiang, Z. H. Lu and C. Yang, *Chem. – Eur. J.*, 2016, **22**, 10860–10866.
11 X. Zeng, K.-C. Pan, W.-K. Lee, S. Gong, F. Ni, X. Xiao, W. Zeng, Y. Xiang, L. Zhan, Y. Zhang, C.-C. Wu and C. Yang, *J. Mater. Chem. C*, 2019, **7**, 10851–10859.
12 K. Wu, T. Zhang, Z. Wang, L. Wang, L. Zhan, S. Gong, C. Zhong, Z. H. Lu, S. Zhang and C. Yang, *J. Am. Chem. Soc.*, 2018, **140**, 8877–8886.
13 K. Wu, Z. Wang, L. Zhan, C. Zhong, S. Gong, G. Xie and C. Yang, *J. Phys. Chem. Lett.*, 2018, **9**, 1547–1553.
14 D. Zhou, D. Liu, X. Gong, H. Ma, G. Qian, S. Gong, G. Xie, W. Zhu and Y. Wang, *ACS Appl. Mater. Interfaces*, 2019, **11**, 24339–24348.
15 H. Nakanotani, T. Higuchi, T. Furukawa, K. Masui, K. Morimoto, M. Numata, H. Tanaka, Y. Sagara, T. Yasuda and C. Adachi, *Nat. Commun.*, 2014, **5**, 1–7.
16 W. Li, Y. Pan, R. Xiao, Q. Peng, S. Zhang, D. Ma, F. Li, F. Shen, Y. Wang, B. Yang and Y. Ma, *Adv. Funct. Mater.*, 2014, **24**, 1609–1614.
17 A. Obolda, Q. Peng, C. He, T. Zhang, J. Ren, H. Ma, Z. Shuai and F. Li, *Adv. Mater.*, 2016, 4740–4746.
18 R. Nagata, H. Nakanotani, W. J. Potscavage and C. Adachi, *Adv. Mater.*, 2018, **30**, 1–6.
19 Q. Zhang, J. Li, K. Shizu, S. Huang, S. Hirata, H. Miyazaki and C. Adachi, *J. Am. Chem. Soc.*, 2012, **134**, 14706–14709.
20 Y. Xu, X. Liang, X. Zhou, P. Yuan, J. Zhou, C. Wang, B. Li, D. Hu, X. Qiao, X. Jiang, L. Liu, S. J. Su, D. Ma and Y. Ma, *Adv. Mater.*, 2019, **31**, 1–8.
21 D. H. Ahn, S. W. Kim, H. Lee, I. J. Ko, D. Karthik, J. Y. Lee and J. H. Kwon, *Nat. Photonics*, 2019, **13**, 540–546.
22 C. Baleizão and M. N. Berberan-Santos, *J. Chem. Phys.*, 2007, **124**, 204510.
23 R. Gómez-Bombarelli, J. Aguilera-Iparraguirre, T. D. Hirzel, D. Duvenaud, D. Maclaurin, M. A. Blood-Forsythe, H. S. Chae, M. Einzinger, D. G. Ha, T. Wu, G. Markopoulos, S. Jeon, H. Kang, H. Miyazaki, M. Numata, S. Kim, W. Huang, S. I. Hong, M. Baldo, R. P. Adams and A. Aspuru-Guzik, *Nat. Mater.*, 2016, **15**, 1120–1127.
24 X. K. Chen, Y. Tsuchiya, Y. Ishikawa, C. Zhong, C. Adachi and J. L. Brédas, *Adv. Mater.*, 2017, **29**, 1–8.
25 D. R. Lee, B. S. Kim, C. W. Lee, Y. Im, K. S. Yook, S. H. Hwang and J. Y. Lee, *ACS Appl. Mater. Interfaces*, 2015, **7**, 9625–9629.
26 Y. J. Cho, K. S. Yook and J. Y. Lee, *Adv. Mater.*, 2014, **26**, 6642–6646.
27 R. Ishimatsu, T. Edura, C. Adachi, K. Nakano and T. Imato, *Chem. – Eur. J.*, 2016, **22**, 4889–4898.
28 Y. J. Cho, K. S. Yook and J. Y. Lee, *Adv. Mater.*, 2014, **26**, 4050–4055.
29 Y. J. Cho, S. K. Jeon, B. D. Chin, E. Yu and J. Y. Lee, *Angew. Chem., Int. Ed.*, 2015, **54**, 5201–5204.
30 C. S. Oh, C. K. Moon, J. M. Choi, J. S. Huh, J. J. Kim and J. Y. Lee, *Org. Electron.*, 2017, **42**, 337–342.
31 C. Tang, T. Yang, X. Cao, Y. Tao, F. Wang, C. Zhong, Y. Qian, X. Zhang and W. Huang, *Adv. Opt. Mater.*, 2015, **3**, 786–790.
32 K. C. Pan, S. W. Li, Y. Y. Ho, Y. J. Shiu, W. L. Tsai, M. Jiao, W. K. Lee, C. C. Wu, C. L. Chung, T. Chatterjee, Y. S. Li, K. T. Wong, H. C. Hu, C. C. Chen and M. T. Lee, *Adv. Funct. Mater.*, 2016, **26**, 7560–7571.
33 H. Sasabe, N. Onuma, Y. Nagai, T. Ito and J. Kido, *Chem. – Asian J.*, 2017, **12**, 648–654.
34 W. Liu, C. J. Zheng, K. Wang, Z. Chen, D. Y. Chen, F. Li, X. M. Ou, Y. P. Dong and X. H. Zhang, *ACS Appl. Mater. Interfaces*, 2015, **7**, 18930–18936.
35 L. Gan, K. Gao, X. Cai, D. Chen and S. J. Su, *J. Phys. Chem. Lett.*, 2018, **9**, 4725–4731.
36 Z. Chen, F. Ni, Z. Wu, Y. Hou, C. Zhong, M. Huang, G. Xie, D. Ma and C. Yang, *J. Phys. Chem. Lett.*, 2019, **10**, 2669–2675.
37 W. Zeng, S. Gong, C. Zhong and C. Yang, *J. Phys. Chem. C*, 2019, **123**, 10081–10086.
38 K. Wang, C. J. Zheng, W. Liu, K. Liang, Y. Z. Shi, S. L. Tao, C. S. Lee, X. M. Ou and X. H. Zhang, *Adv. Mater.*, 2017, **29**, 1–9.
39 W. Li, X. Cai, B. Li, L. Gan, Y. He, K. Liu, D. Chen, Y. C. Wu and S. J. Su, *Angew. Chem., Int. Ed.*, 2019, **58**, 582–586.
40 K. Masui, H. Nakanotani and C. Adachi, *Org. Electron.*, 2013, **14**, 2721–2726.

